A Comparative Study on the Pollutant Removal Efficiency of $CoFe_2O_4$@ HKUST-1 MOF and $CoFe_2O_4$ Nanoparticles

Tahoura Saemian[1,2] · Mehrnaz Gharagozlou[1] (ORCID) · Moayad Hossaini Sadr[2,3] · Sanaz Naghibi[4]

Abstract

In this work, $CoFe_2O_4$ nanoparticles were fabricated by the Pechini sol–gel technique. Then, $Cu_3(BTC)_2$ or HKUST-1 metal–organic framework was used to prepare Co-ferrite@HKUST-1 composite. The as-synthesized composite powder and Co-ferrite nanoparticles were compared by their performance for methyl orange (MO) and methylene blue (MB) degradation. X-ray diffractometry (XRD), transmission electron microscopy (TEM), scanning electron microscopy (SEM), and vibrating sample magnetometer (VSM) were utilized to evaluate the as-prepared samples. Results showed that the average grain size was about 20–30 nm. The magnetic saturation value for Co-ferrite nanoparticles and Co-ferrite@HKUST-1 composite were 65 and 20 emu/g, respectively. Results of the removal efficiency of the Co-ferrite samples approved that just the cation dyes concentrations decreased, whereas in the case of the Co-ferrite@HKUST-1 composite samples both anionic and cationic organic dyes were degraded efficiently.

Keywords Co-ferrite · $Cu_3(BTC)_2$ · Co-ferrite@HKUST-1 · Magnetic compound · Catalytic performance

1 Introduction

Human activities since the advent of the industrial revolution have generated a deeply negative impact on the Earth's ecosystem. Currently, nearly half of the world's population is living in water-stressed areas, and it is projected to get worse in the following decades with the increase in global temperatures as a consequence of global warming. Providing universal access to clean freshwater is one of the main goals of the governments. Organic pollutants are by their diversity, in nature and as a source of contamination, a more wide family than inorganic contaminants [1]. Dyes, detergents, oils, polyaromatic hydrocarbons, pesticides/insecticides/herbicides and pharmaceuticals, and personal care products (PPCPs) are some of the most common organic contaminants found in water streams [2]. Methyl orange is one of the well-known acidic/anionic dyes and has been widely used in textile, printing, paper, food and pharmaceutical industries and research laboratories and methylene blue is one of the most common dying materials for wood, silk, and cotton so and the removal of MO and MB from water is very important due to their toxicity [3].

Various treatment techniques including physical, biological, chemical and electrochemical methods as well as a combination of these techniques for removing organic dyes from wastewater have been reported and reviewed in the literature. Biological treatment is commonly used for the removal of organic pollutants from textile wastewater. These methods are environmentally friendly, produce less sludge, and are relatively inexpensive [4, 5]. However, the application of these techniques may be limited by their needs for a large

✉ Mehrnaz Gharagozlou
gharagozlou@icrc.ac.ir

Tahoura Saemian
t.saemian@azaruniv.edu

Moayad Hossaini Sadr
hosainis@yahoo.com

Sanaz Naghibi
naghibi@iaush.ac.ir

1 Department of Nanomaterials and Nanocoatings, Institute for Color Science and Technology, PO. Box 1668814811, Tehran, Iran

2 Department of Chemistry, Faculty of Science, Azarbaijan Shahid Madani University, Tabriz, Iran

3 Ascotec Holding GMBH, Tersteegenstrasse 10, 40474 Dusseldorf, Germany

4 Department of Metallurgy and Materials Engineering, Shahreza Branch, Islamic Azad University, PO. Box 311–86145, Shahreza, Iran

land area, very slow treatment process and the presence of recalcitrant toxic organic dyes. Physicochemical methods such as adsorption by activated carbon and nanostructured porous metal–organic framework materials [6, 7], chemical methods such as ozonation [8], and UV assisted advanced oxidation and dielectric discharge in a falling liquid film [9, 10] are widely used for the removal of organic dyes from aqueous solution. Also recently, magnetic loaded adsorbent materials have gained special attention in water purification, based on their numerous advantages such as high separation efficiency, simple manipulation process, kind operation conditions and easy specifically functional modifications [11, 12].

Magnetic adsorbents should be utilized in the magnetic separation method. After the adsorption procedure, the magnetic adsorbents could be easily collected from wastewater via an external magnetic field. This method is an efficient, fast and economical procedure for the separation of magnetic compounds from the medium after the adsorption treatment of pollutants [13]. Furthermore, magnetic separation provides a suitable route for online separation [14]. Ferrites of the form MFe_2O_4 commonly include metal cations such as Ba^{2+} [15], Cu^{2+} [16], Mg^{2+} [17], Fe^{2+} [18], Sr^{2+} [19], Ni^{2+} [18], Zn/Ni/Fe [20], Mg/Cu/Zn [21], and Zn^{2+} [22]. $CoFe_2O_4$ is classified in this category and shows some specific characteristics which make it interesting for different research groups [23–25].

The most widely used catalytic process for dyes decolorization is Fenton oxidation, and several modification methods were introduced to improve its performance [26, 27], such as using some metal ligands [28, 29]. Recently, several coppers and cobalt-based Fenton-like systems for homogeneous catalytic decomposition of hydrogen peroxide and production of hydroxyl radicals were described. They take advantage of simple organic molecules, such as organic acids or amino acids, to increase the oxidative performance of Cu/H_2O_2 to degrade synthetic dyes or nonpolar organic compounds [30–32].

Baldrian et al. have shown that ferrites can be effective in Fenton-type systems at neutral to basic pH. It has been seen that the production of OH^- from H_2O_2 can be effective at pH 4–8 for $MnFe_2O_4$, $CuFe_2O_4$, $CoFe_2O_4$, and Fe_3O_4 [25]. In certain cases, the effective pH range can be extended even further, for example, $CuFe_2O_4$ and $CoFe_2O_4$ still produce OH^- up to pH 12 and $MnFe_2O_4$ remains effective at a pH of 2. This is a large improvement over the normal limiting acidic conditions needed (pH 2–4) for traditional Fenton systems [33]. On the other hand surface coating of nanoparticles with various materials to form core–shell morphologies is often used for the development of catalysts [34]. Moreover, metal–organic frameworks (MOFs) are an emerging class of coordination networks, or porous coordination polymers (PCPs), consisting of two main components: a metal ion or

cluster of metal ions and an organic molecule called a linker. The choice of metal and linker has a significant impact on the structure and characteristics of the MOF [35]. During recent years, intensive interest has been aroused in the catalytic properties of MOFs [36]. Furthermore, under light irradiation, the bridging linkers of MOFs can serve as antennas to harvest photons and activate the metal nodes [37], or the metal oxide clusters of MOFs can be directly excited by absorbing photons [38]. This can induce the charge transition either between linker and metal cluster or within metal oxide cluster itself, and illustrate the semiconductor-like behavior. Therefore, based on their catalytically active metals/organic linkers [39–41].

In this study, for the first time, $CoFe_2O_4$ nanoparticles composed to the $Cu_3(BTC)_2$ metal–organic framework were introduced as an adsorbent and to the removal of organic dyes. MO and MB solutions were selected in this study as a representative acidic (anionic) dye and basic (cationic) dye, respectively. Then the experiments were conducted to compare the removal efficiencies of MO or MB by $CoFe_2O_4$ and $CoFe_2O_4$@HKUST-1 compound. This compound could be classified as an engineering material due to its possible applications in different fields due to its specific characteristics such as high specific surface area and adsorption capability, strong magnetic behavior, and non-toxic nature. These properties could make this compound as a candidate for further investigation.

2 Experimental Procedures

2.1 Starting Chemicals

Iron nitrate ($Fe(NO_3)_3 \cdot 9H_2O$), cobalt nitrate ($Co(NO_3)_2 \cdot 6H_2O$), citric acid, ethylene glycol, trimesic acid ($C_6H_3(CO_2H)_3$, benzene-1,3,5-tricarboxylic acid: H_3BTC), copper nitrate ($Cu(NO_3)_2 \cdot 3H_2O$), thioglycolic acid ($HSCH_2CO_2H$, or mercaptoacetic acid: MAA), methylene blue (MB), methyl orange (MO), hydrogen peroxide and ethanol were purchased from Merck and used as received without any further treatment. Deionized water obtained from a system was used to prepare aqueous solutions for $CoFe_2O_4$ and $CoFe_2O_4$@$Cu_3(BTC)_2$ synthesize and for the catalytic removal experiments.

2.2 $CoFe_2O_4$ Preparation

$CoFe_2O_4$ nanoparticles were synthesized by Pechini sol–gel method. In this procedure, 309 mmol citric acid was added to 14 mmol of deionized water and stirred for 10 min. 63 mmol $Fe(NO_3)_3 \cdot 9H_2O$ and 32 mmol $Co(NO_3)_2 \cdot 6H_2O$ had been separately dispersed in 0.6 mmol deionized water and stirred using magnetic stirrer for 30 min. In this study,

the molar ratio $Co(NO_3)_2 \cdot 6H2O$: $Fe(NO_3)_3 \cdot 9H_2O$ was kept constant at 1:2. 41.58 mL ethylene glycol was added to the above solution slowly and stirred for 4 h at 90 °C. The sols were allowed to gel at room temperature for 7 days in partially closed glass vessels. The obtained alcogel was dried at 300 °C for 2 h then fired at 500 °C with a heating rate of 10 °C/min.

2.3 Synthesis of CoFe$_2$O$_4$@HKUST-1 Nanocomposite

0.51 g the obtained powder and 0.02 mL MAA were added to 100 mL ethanol and stirred for 24 h at room temperature. The product was summed by an external magnetic field and washed three times with deionized water and ethanol. Then, 0.2 g of the prepared compound and 7.5 mmol $Cu(NO_3)_2 \cdot 3H_2O$ were added to 100 mL ethanol. 4.1 mmol H_3BTC was dissolved in 100 mL of ethanol, separately, and added dropwise to the first solution under vigorous agitation for 2 h. The prepared compound was collected by an external magnetic field and washed three times with deionized water, as well as ethanol, then dried at 70 °C.

2.4 Evaluation of Dye-Removing Activity Activities

The degradation experiments were performed in an aqueous solution containing MB or MO. In the beginning, MO and MB solutions with a concentration of 20 mg/L were prepared. Then, 0.1 mmol H_2O_2 was added to each solution. 40 mg Co-ferrite powder or 10 mg Co-ferrite@HKUST-1 compound were added to the solutions to evaluate the dye-removing performances of the samples. Ultrasonic irradiation with the power of 400 W was utilized to disperse the as-synthesized compounds in the solutions. After a while, magnetic particles were separated using an external magnet. The concentrations of dyes were measured by a UV–Visible spectrophotometer at the wavelength of 200–800 nm (Perkin Elmer device). This procedure was designed to evaluate the dye-removing performance through adsorption but not via catalytic activity.

2.5 Characterization

X-ray diffraction (XRD) data were recorded by a Philips PNA analytical device. Based on the resulted data, crystallite size was calculated from broadening of XRD peaks using the Williamson–Hall Equation, where B, θ, λ, d, and η are the peak full width at half maximum (FWHM), diffraction angle, wavelength of the X-ray, crystallite size, and lattice strain, respectively [42]. Scanning electron microscopy (SEM) and transmission electron microscopy (TEM) analyses were conducted by an LEO 1455VP device and a Philips 200 FEG device, respectively. FTIR spectra in the range of 400–4000 cm^{-1} were recorded on a Perkin Elmer Spectrum
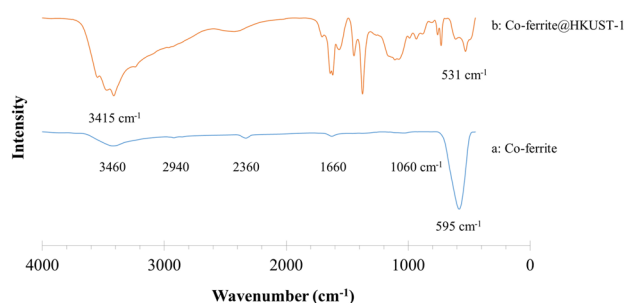

Fig. 1 FTIR spectra of a Co-ferrite and b Co-ferrite@HKUST-1 samples

Table 1 Frequencies and assignments of FTIR bands of the Co-ferrite and Co-ferrite@HKUST-1 samples

Sample	IR frequencies (cm^{-1})	Assignment	Related compound
CoFe$_2$O$_4$	595 S	υ Co–O and Fe–O	CoFe$_2$O$_4$
	1060 W	υ C–O	Alcohol
	1660 W	υ C=C	Aromatic ring
	2360 W	–	Atmospheric CO$_2$
	2940 W	υ C–H	Alkane
	3460 W	υ O–H	H$_2$O
Co-ferrite@ HKUST-1	531 M	υ Co–O and Fe–O	CoFe$_2$O$_4$
	731 M	δ =C–H	Alkene
	760 W	δ =C–H	Alkene
	934 W	δ =C–H	Alkene
	990 W	δ =C–H	Alkene
	1110 M	υ C–O	Alcohol
	1375 S	δ –C–H	Alkane
	1445 M	υ C=C	Aromatic ring
	1567 M	υ C=O	Aromatic ring
	1619 S	υ C=C	Alkene
	1640 S	υ C=O	Amide
	2428 W	–	Atmospheric CO$_2$
	3415 S	υ O–H	H$_2$O

υ stretching vibration, δ bending vibration

One spectrophotometer with KBr pellets. The magnetization curves were measured at room temperature under a varying magnetic field from − 10.000 to 10.000 oe by a BHV-55 vibrating sample magnetometer (VSM).

$$B \cdot \cos(\theta) = (0.9\lambda/d) + \eta \cdot \sin(\theta) \qquad (1)$$

3 Results and Discussion

3.1 FTIR Spectroscopy

Figure 1 shows the FTIR spectra of Co-ferrite (a) and Co-ferrite@HKUST-1 (b) samples and the IR peaks and their assignments are summarized in Table 1. According to

Fig. 1a, the main peak occurred at 595 cm^{-1} and is related to the vibrations of Co–O and Fe–O bond in the Co-ferrite nanoparticles. The other 3 week peaks localized at 1060, 1660, and 2940 are related to the C–O, C=C, and C–H stretching vibration bands, respectively. These events could originate from organic materials that were used during Co-ferrite syntheses, such as MAA. A tiny peak at 2360 cm^{-1} maybe refers to the atmospheric CO^2 gas. Finally, a week peak at 3460 cm^{-1} is related to the surface water.

Based on Fig. 1b, Co-ferrite@HKUST-1 nanocomposite contains some absorption peaks, which are listed in Table 1. The first one at 531 cm^{-1} is due to vibrations of Co–O and Fe–O in Co-ferrite. Four peaks at the frequency range of 700–1000 cm^{-1} are related to bending=C–H vibration and one peak at 1619 cm^{-1} is assigned to the stretching C=C vibration. These events may originate from alkene functional groups. Furthermore, a peak with medium intensity at 1110 could be related to stretching C–O vibration and originated from alcohol. There is a strong peak at 1375 cm^{-1}, which is related to the bending –C–H vibration and may be originated from an alkane functional group. Two peaks with medium intensity at 1445 and 1567 cm^{-1} are attributed to the stretching C=C and C=O vibration, respectively. Both of them could be originated from aromatic rings. Observation of a peak at 1640 cm^{-1} is not routine in such a compound. Although this maybe refers to the stretching C=O vibration, the originate of such a vibration is an amide. The origination of the two last peaks has been disused before. However, a comparison between FTIR spectra of the synthesized HKUST-1 [43] and this composite compound approved the existence of HKUST-1 in the as-synthesized compound.

3.2 Phase Component and Morphology

Figure 2a shows XRD patterns of the synthesized samples, CoFe$_2$O$_3$ and CoFe$_2$O$_4$@HKUST-1. According to Fig. 2a, the XRD peaks at $2\theta = 8.08°$ (111), 11.06° (220), 13.00° (311), 15.92° (222), 18.17° (400), 20.20° (422), 23.44° (333) are match well with the standard XRD data for the cubic spinel phase and Fd3 m (2 2 7) space group of CoFe$_2$O$_3$ (JCPDS: 22-1086). This phase has been formed without any additional peak or impurity. Figure 2b shows that the diffraction pattern of CoFe$_2$O$_4$@HKUST-1 compound consists of the CoFe$_2$O$_3$ diffraction peaks and also those of the Cu$_3$(BTC)$_2$ compound (JCPDS: 1-276). Weakening and thickening of the crystalline Co-ferrite plates and Cu$_3$(BTC)$_2$ were observed, and the reduction of peaks intensity and their expansion could be due to the reduction of crystallite size in the nanocomposite compared to CoFe$_2$O$_4$ and Cu$_3$(BTC)$_2$.

Figure 3 shows SEM and TEM images of the as-synthesized Co-ferrite and Co-ferrite@HKUST-1 compounds. The SEM images of both samples showed that the morphologies of particles were almost semi-spherical, and dispersed
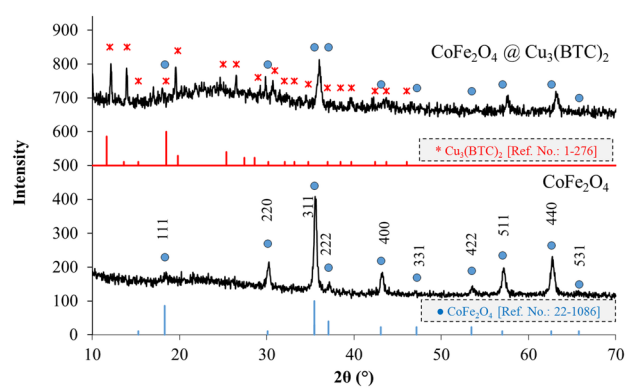

Fig. 2 XRD patterns of a Co-ferrite and b Co-ferrite@HKUST-1 samples

unevenly. On the other hand, Co-ferrite nanoparticles have a size of about 25–35 nm. TEM images of the Co-ferrite@HKUST-1 sample exhibited no significant changes in the particle size compared with that of the Co-ferrite sample. Another point that should be noticed is that the as-synthesized particles are agglomerated. This might originates from residual polymeric materials covering particles and resulting in agglomeration. However, TEM images approved that the average particle size of the synthesized composite compound is about 30 nm. For further study, the average crystallite sizes of the samples, based on the Williamson–Hall technique, were calculated about 24 nm, which is in good agreement with TEM observation.

3.3 VSM

Figure 4 shows the hysteresis curves of the synthesized compounds; HKUST-1, Co-ferrite, and Co-ferrite@HKUST-1. Although the magnetic saturation of the Co-ferrite powder and HKUST-1 compound were about 65 and 0 emu/g, respectively, the ferromagnetic characteristic of the Co-ferrite@HKUST-1 compound was measured about 20 emu/g. The importance of this achievement would be clear when the magnetization values of other compounds are studied. The reported values are about 1.5 [44] and 15 [45] emu/g for Fe$_3$O$_4$@HKUST-1, and 30 emu/g for Cu-CuFe$_2$O$_4$@HKUST-1 [46].

3.4 The Effect of the Different Synthesized Samples on the Removal of MO and MB Solutions

The effects of different samples on the removal of MO and MB solutions were studied to evaluate the surface charge of the powder samples. Figs. 5, 6; Table 2 represent the results of MB and MO degradation due to the existence of the synthesized particles.
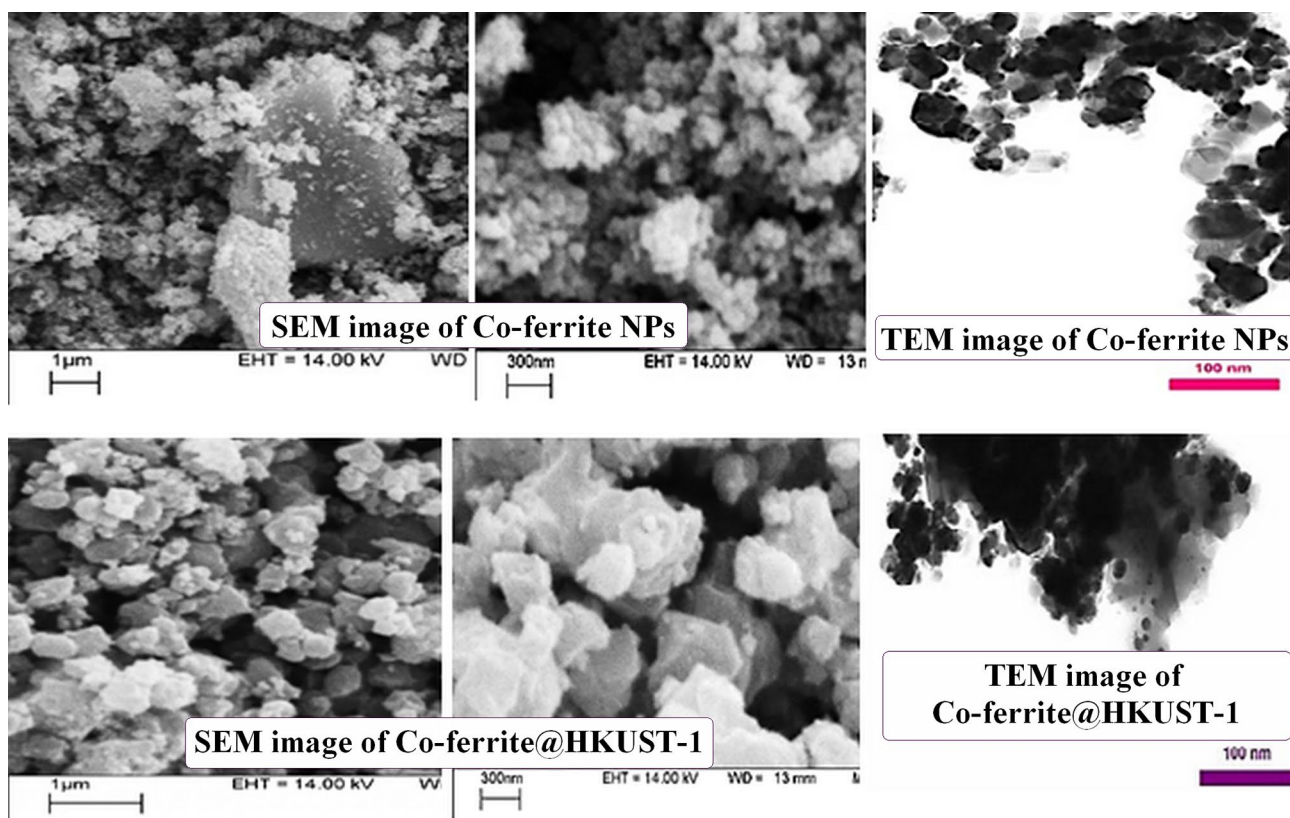
Fig. 3 SEM and TEM images of Co-ferrite and Co-ferrite@HKUST-1 samples
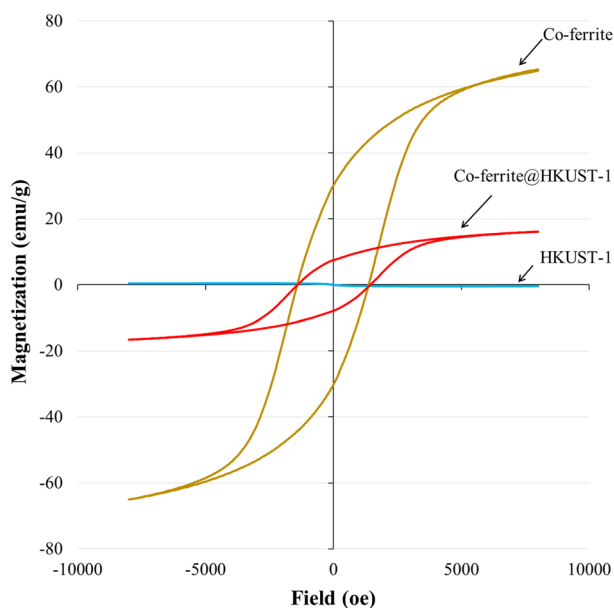

Fig. 4 Magnetic saturation of Co-ferrite, HKUST-1, and Co-ferrite@HKUST-1 samples

As can be seen, in the presence of the Co-ferrite powder (see Fig. 5a; Table 2), the removal efficiency of MB after 100 min was about 94%. This is due to the positive charges of MB molecules in the neutral pH, which could facilitate the adsorption process due to the negative surface charge of the HKUST-1 particles. On the other hand, more than 95% of the MO degradation occurred after 100 min in the acidic pH (see Fig. 5b; Table 2). These results suggest that the surface of Co-ferrite is probably anionic in aqueous solution, however, it should also be noted that the presence of Co-ferrite, H_2O_2, and acidic pH was necessary to generate the Fenton phenomenon for the removal of MO dyes.

In the presence of the Co-ferrite@HKUST-1 compound (see Fig. 6a; Table 2), the removal efficiency of MO dye was about 90% after 210 min in Neutral pH, which is less than the Co-ferrite efficiency. Therefore, in comparison with the Co-ferrite@HKUST-1 compound, more amount of Co-ferrite is required to remove MO and Co-ferrite@HKUST-1 removal efficiency is higher than that of the Co-ferrite sample. Accordingly, the higher performance of Co-ferrite@HKUST-1 in comparison to Co-ferrite can be related to the presence of the active sites of Co-ferrite in the matrix of the modified adsorbent and its higher capacity [47].
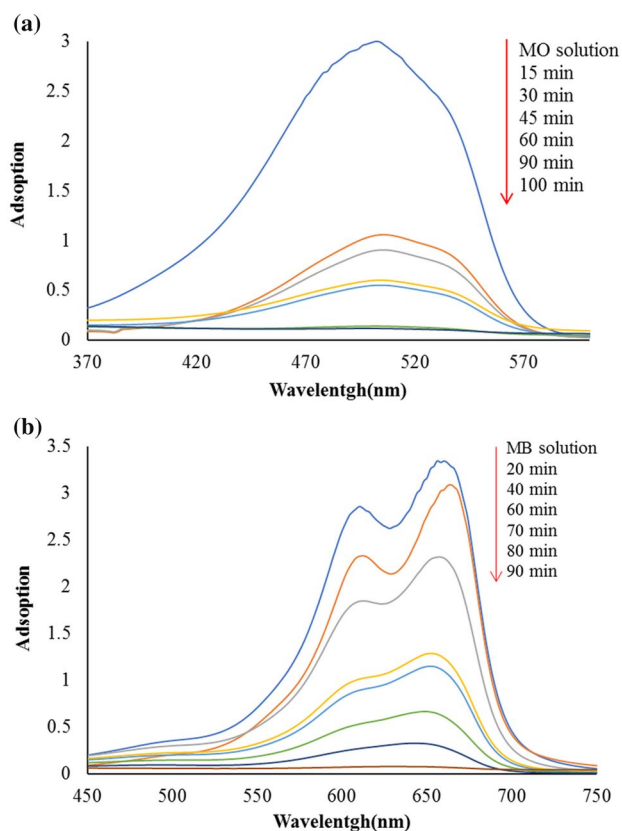
(a)

(b)

Fig. 5 The variation of UV–visible absorption spectra for **a** MO and **b** MB dyes (20 mg/L) in the present of Co-ferrite nanoparticles (40 mg/L)

A comparison between the observed results with other works approved that the removal efficiency of the as-synthesized Co-ferrite@HKUST-1 compound is as high as that of HKUST-1/graphite oxide [48] and Fe_3O_4@HKUST-1 [45].

3.5 The Effects of Dye Concentration on the Removal Efficiency

Figure 6 shows the influences of the dye concentration on the dye removal efficiency in the presence of the Co-ferrite@HKUST-1 compound. The experiment of the initial dye concentration was carried out in two dye concentrations; 10 and 20 mg/L, pH of 6, and the addition of 10 mL H_2O_2 to 100 mL of the dye solution. It is clear that with an increase in the initial dye concentration from 10 to 20 mg/L, the removal of dye was reduced from 93% to about 90% at 210 min. This can be attributed to the fact that the active sites on the adsorbent for dye removal decrease when the dye concentration increased.
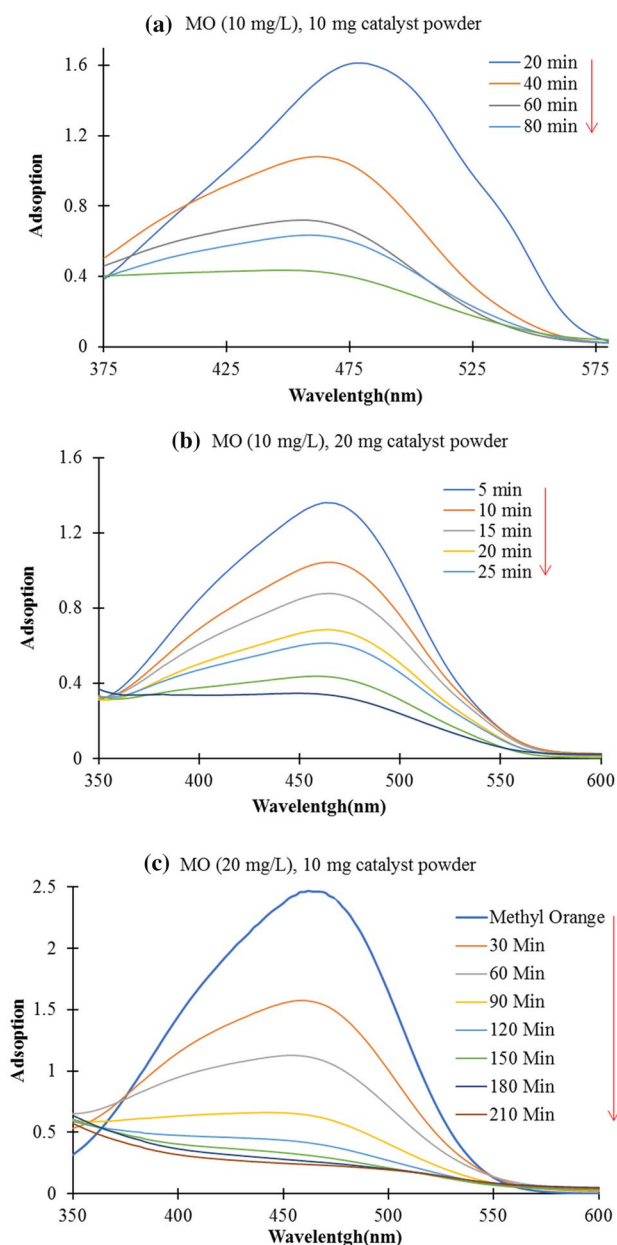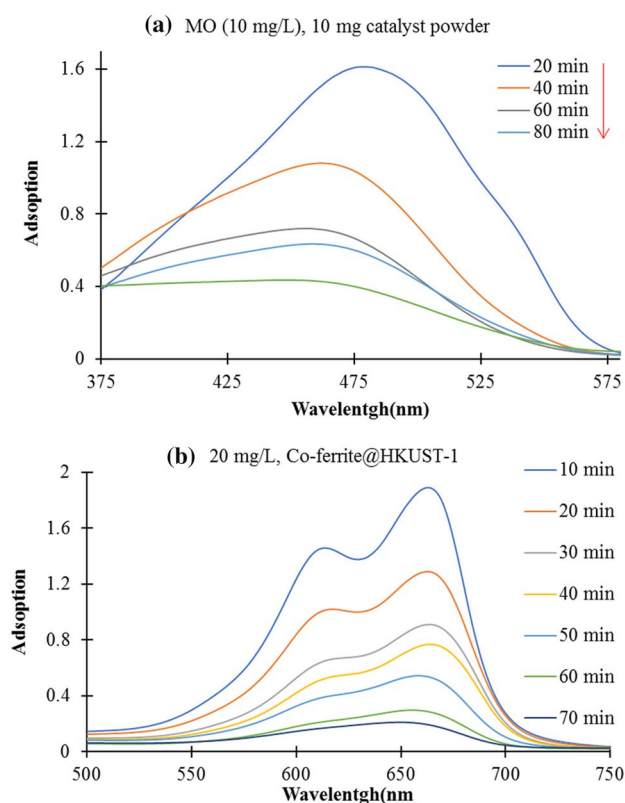
(a) MO (10 mg/L), 10 mg catalyst powder

(b) MO (10 mg/L), 20 mg catalyst powder

(c) MO (20 mg/L), 10 mg catalyst powder

Fig. 6 The variation of UV–visible absorption spectra for MO dye. **a** and **b** synthesized powder dosage-dependent, **c** dye concentration-dependency in the present of Co-ferrite@HKUST-1 sample

3.6 The Effects of Co-ferrite@HKUST-1 Composite Dosage on the Removal Efficiency

Figure 7 showed the impacts of Co-ferrite@HKUST-1 concentration of the removal efficiency. This effect was evaluated under certain conditions in which the pH value was adjusted at 6 and 10 mL H_2O_2 was added to 100 mL dye solution. Increasing 10 cyclethe concentration of the Co-ferrite@HKUST-1 from 10 to 20 mg/L led to an increase in removal efficiency. The removal efficiencies

Table 2 The effects of the Co-ferrite and Co-ferrite@HKUST-1 samples on the removal of dye solutions

Sample	Dye	Dye concentration (mg/L)	Synthesized powder concentration (mg/L)	pH	Time (min)	R (%)
Co-ferrite	MO	20	40	3	100	95
	MB			6		94
Co-ferrite@ HKUST-1	MO	20	40	6	210	90
		10	10	6	90	93
			20	6	35	80
				3	75	78
	MB		10	6	135	97
				6	70	90
			20	9	15	91

Fig. 7 The variation of UV–visible absorption spectra for MB dye (10 mg/L), synthesized powder dosage-dependent in the presence of Co-ferrite@HKUST-1 sample

of MO in the presence of synthesized powder with the concentration of 10 or 20 g/L were about 93 and 80%, respectively. In the case of MB, these values were about 99.8 and 90%, respectively. These results showed that the solution with the higher concentration would provide a high enough surface area and more operational adsorption traps. Comparing the influence of synthesized powder amount on the removal of MO or MB demonstrated the excellent removal efficiency by the optimum dosage of the magnetic nanocomposite.

3.7 The Effects of Alkaline pH on the Removal Efficiency by the Co-ferrite@HKUST-1

The pH value is one of the most significant variables influencing the adsorption behavior. An appropriate pH value can improve the adsorption efficiency, and reduce interference from the matrix. NaOH or HCl was used to adjust pH values. The pH of the MO solution as an anionic dye was set on 3 because the positive charge on the particles surface will increase. On the other hand, electrostatic attraction between the negative surface charge of MO and positive surface charge of the adsorbent will increase, too. The pH of the MB solution as a cationic dye was set on 9. Based on Fig. 8, the removal efficiency of MO dye by Co-ferrite@HKUST-1 (20 mg/L) in pH 3 was 78% after 75 min, and the removal efficiency of MB dye in pH 9 was 88% after 15 min.

3.8 Stability of Co-Ferrite@HKUST-1

Figure 9 shows the FTIR evaluation results of the Co-ferrite@HKUST-1 samples before and after 10 cycles of the decolorization process. As can be seen, the main peaks of this compound at 530 cm^{-1} (attributed to the Fe–O and Co–O stretch mode) and at 1142, 1784, 1719 cm^{-1} (assigned to $Cu_3(BTC)_2$ vibrations) remained unchanged, indicating that there was no change in the molecular structure of the Co-Ferrite@HKUST-1 samples before and after catalytic reactions. These results confirmed that the Co-Ferrite@HKUST-1 compound was stable in aqueous solution, and could be used circularly.

4 Conclusion

In this work, Co-Ferrite@HKUST-1 nanocomposite was prepared by a novel method and used as an efficient magnetically separable environmental compound for decolorization of various dyes. Moreover, the magnetic saturation extent for Co-ferrite particles and Co-ferrite@HKUST-1 samples were
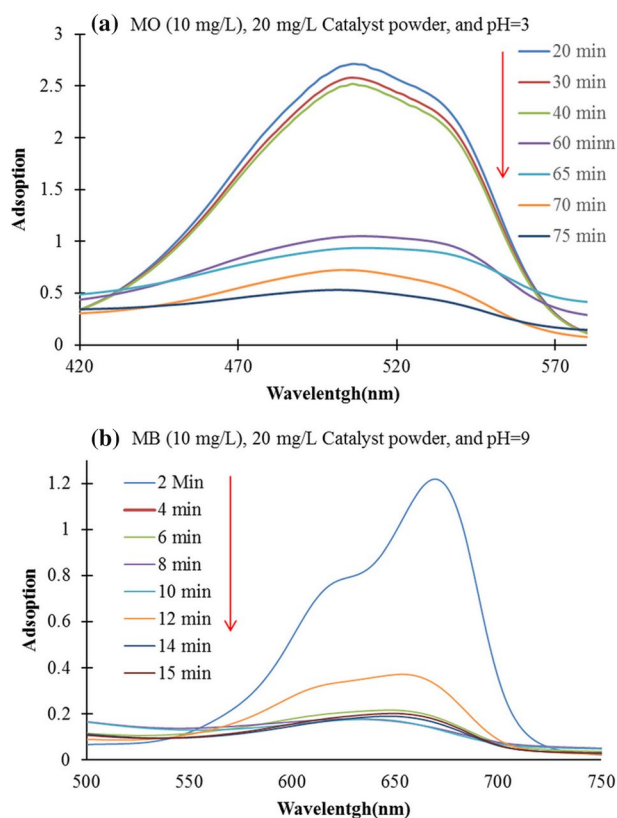
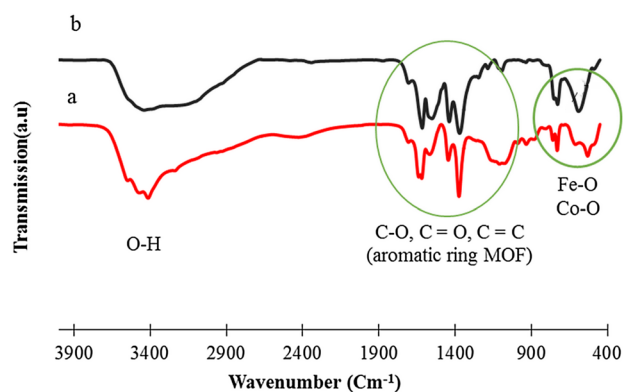**Fig. 8** The variation of UV–visible absorption spectra for **a** MO and **b** MB dyes in different pH values

Fig. 9 FTIR spectra of a Co-ferrite@HKUST-1; b Co-ferrite@HKUST-1 after 10 cycle decolorization process

surface and generates an electrostatic attraction between anionic dyes and particles surface. Also, the Co-ferrire@HKUST-1 compound seems to be more positive than Co-Ferrite, because the cationic dyes were removed in neutral pH. Finally, different removal efficiencies approved that the Co-ferrite nanoparticles had good properties for the removal of cationic dyes, and Co-ferrite@HKUST-1 composite was a good candidate for removal of organic dyes existed in aqueous solutions.

References

1. L. Xu, *Impact of climate change and human activity on the eco-environment: an analysis of the Xisha Islands* (Springer, Berlin, 2014), pp. 35–55
2. M. Mon, R. Bruno, J. Ferrando-Soria, D. Armentano, E. Pardo, J. Mater. Chem. A **6**, 4912–4947 (2018)
3. E. Haque, J.W. Jun, S.H. Jhung, J. Hazard. Mater. **185**, 507–511 (2011)
4. M. Kornaros, G. Lyberatos, J. Hazard. Mater. **136**, 95–102 (2006)
5. M. Solís, A. Solís, H.I. Pérez, N. Manjarrez, M. Flores, Process Biochem. **47**, 1723–1748 (2012)
6. K.P. Singh, D. Mohan, S. Sinha, G.S. Tondon, D. Gosh, Ind. Eng. Chem. Res. **42**, 1965–1976 (2003)
7. A. Ayati, M.N. Shahrak, B. Tanhaei, M. Sillanpää, Chemosphere **160**, 30–44 (2016)
8. A.R. Tehrani-Bagha, N.M. Mahmoodi, F.M. Menger, Desalination **260**, 34–38 (2010)
9. B.P. Dojčinović, G.M. Roglić, B.M. Obradović, M.M. Kuraica, M.M. Kostić, J. Nešić, D.D. Manojlović, J. Hazard. Mater. **192**, 763–771 (2011)
10. K.H.H. Aziz, A. Mahyar, H. Miessner, S. Mueller, D. Kalass, D. Moeller, I. Khorshid, M.A.M. Rashid, Process Saf. Environ. Prot. **113**, 319–329 (2018)
11. R.D. Ambashta, M. Sillanpää, J. Hazard. Mater. **180**, 38–49 (2010)
12. Y.-J. Liu, S.-S. Guo, Z.-L. Zhang, W.-H. Huang, D. Baigl, M. Xie, Y. Chen, D.-W. Pang, Electrophoresis **28**, 4713–4722 (2007)
13. S. Wang, Y.-Y. Zhai, Q. Gao, W.-J. Luo, H. Xia, C.-G. Zhou, J. Chem. Eng. Data **59**, 39–51 (2014)
14. T. Madrakian, A. Afkhami, H. Ahmadi, H. Bagheri, J. Hazard. Mater. **196**, 109–114 (2011)
15. Y. Yang, Y. Jiang, Y. Wang, Y. Sun, L. Liu, J. Zhang, Mater. Chem. Phys. **105**, 154–156 (2007)
16. E. Manova, T. Tsoncheva, D. Paneva, M. Popova, N. Velinov, B. Kunev, K. Tenchev, I. Mitov, J. Solid State Chem. **184**, 1153–1158 (2011)
17. L. Zhang, X. Zhou, X. Guo, X. Song, X. Liu, J. Mol. Catal. A **335**, 31–37 (2011)
18. D. Guin, B. Baruwati, S.V. Manorama, J. Mol. Catal. A **242**, 26–31 (2005)
19. S.K. Pardeshi, R.Y. Pawar, J. Mol. Catal. A **334**, 35–43 (2011)
20. A. Ghasemi, M.R. Loghman-Estarki, S. Torkian, M. Tavoosi, Compos. B Eng. **175**, 107179 (2019)
21. M.R. Loghman-Estarki, S. Torkian, R.A. Rastabi, A. Ghasemi, J. Magn. Magn. Mater. **442**, 163–175 (2017)
22. X. Li, Y. Hou, Q. Zhao, L. Wang, J. Colloid Interface Sci. **358**, 102–108 (2011)
23. E. Manova, T. Tsoncheva, D. Paneva, I. Mitov, K. Tenchev, L. Petrov, Appl. Catal. A **277**, 119–127 (2004)
24. S. Zhang, H. Niu, Y. Cai, X. Zhao, Y. Shi, Chem. Eng. J. **158**, 599–607 (2010)

special for ferromagnetic compounds. The catalytic properties of Co-ferrite@HKUST-1 compound were evaluated by decolorization of different dyes. The results and observations showed that the as-prepared Co-Ferrite@HKUST-1 composite improved the catalytic activity compared to the Co-ferrite nanoparticles. It seems that the Co-Ferrite surface was negatively charged due to the removal of anionic dyes in pH 3. This creates a positive charge on the particles

25. P. Baldrian, V. Merhautová, J. Gabriel, F. Nerud, P. Stopka, M. Hrubý, M.J. Beneš, Appl. Catal. B **66**, 258–264 (2006)
26. J. Perkowski, L. Kos, S. Ledakowicz, Ozone Sci. Eng. **18**, 73–85 (1996)
27. K. Dutta, S. Bhattacharjee, B. Chaudhuri, S. Mukhopadhyay, J. Environ. Sci. Health Part A **38**, 1311–1326 (2003)
28. B. Goodell, Y. Qian, J. Jellison, M. Richard, Water Environ. Res. **76**, 2703–2707 (2004)
29. S. Nam, V. Renganathan, P. Tratnyek, Chemosphere **45**, 59–65 (2001)
30. F. Nerud, P. Baldrian, J. Gabriel, D. Ogbeifun, Chemosphere **44**, 957–961 (2001)
31. V. Shah, P. Verma, P. Stopka, J. Gabriel, P. Baldrian, F. Nerud, Appl. Catal. B **46**(2), 287–292 (2003)
32. J. Gabriel, P. Baldrian, P. Verma, T. Cajthaml, V. Merhautová, I. Eichlerová, I. Stoytchev, T. Trnka, P. Stopka, F. Nerud, Appl. Catal. B **51**, 159–164 (2004)
33. E. Casbeer, V.K. Sharma, X.-Z. Li, Sep. Purif. Technol. **87**, 1–14 (2012)
34. F.A. Harraz, R.M. Mohamed, M.M. Rashad, Y.C. Wang, W. Sigmund, Ceram. Int. **40**, 375–384 (2014)
35. B. Soltani, H. Nabipour, N.A. Nasab, J. Inorg. Organomet. Polym Mater. **28**, 1090–1097 (2018)
36. H. Deng, S. Grunder, K.E. Cordova, C. Valente, H. Furukawa, M. Hmadeh, F. Gándara, A.C. Whalley, Z. Liu, S. Asahina, H. Kazumori, M. O'Keeffe, O. Terasaki, J.F. Stoddart, O.M. Yaghi, Science **336**, 1018–1023 (2012)
37. A.H. Chughtai, N. Ahmad, H.A. Younus, A. Laypkov, F. Verpoort, Chem. Soc. Rev. **44**, 6804–6849 (2015)
38. M.A. Nasalevich, M. van der Veen, F. Kapteijn, J. Gascon, CrystEngComm **16**, 4919–4926 (2014)
39. D. Wang, R. Huang, W. Liu, D. Sun, Z. Li, ACS Catal. **4**, 4254–4260 (2014)
40. T. Zhang, W. Lin, Chem. Soc. Rev. **43**, 5982–5993 (2014)
41. J. Tu, X. Zeng, F. Xu, X. Wu, Y. Tian, X. Hou, Z. Long, Chem. Commun. **53**, 3361–3364 (2017)
42. M. Gharagozlou, S. Naghibi, J. Chin. Chem. Soc. **63**, 290–297 (2016)
43. Saemian T, Gharagozlou M, Hosseini Sadr M, Naghibi S (2019) Polyhedron 114163
44. T. Toyao, M.J. Styles, T. Yago, M.M. Sadiq, R. Riccò, K. Suzuki, Y. Horiuchi, M. Takahashi, M. Matsuoka, P. Falcaro, CrystEngComm **19**, 4201–4210 (2017)
45. X. Zhao, S. Liu, Z. Tang, H. Niu, Y. Cai, W. Meng, F. Wu, J.P. Giesy, Sci. Rep. **5**, 11849 (2015)
46. S. Fan, W. Dong, X. Huang, H. Gao, J. Wang, Z. Jin, J. Tang, G. Wang, ACS Catal. **7**, 243–249 (2017)
47. T. Zhang, X. Zhang, X. Yan, L. Kong, G. Zhang, H. Liu, J. Qiu, K.L. Yeung, Chem. Eng. J. **228**, 398–404 (2013)
48. L. Li, X.L. Liu, H.Y. Geng, B. Hu, G.W. Song, Z.S. Xu, J. Mater. Chem. A **1**, 10292–10299 (2013)